

Computationally efficient description of relativistic electron beam transport in collisionless plasma

Oleg Polomarov

*Department of Physics and Institute for Fusion Studies, The University of Texas at Austin,
Austin, Texas 78712*

Adam B. Sefkow and Igor Kaganovich

Plasma Physics Laboratory, Princeton University, Princeton, New Jersey 08543

Gennady Shvets

*Department of Physics and Institute for Fusion Studies, The University of Texas at Austin,
Austin, Texas 78712*

(Received 28 July 2006; accepted 24 January 2007; published online 18 April 2007)

A reduced approach to modeling the electromagnetic Weibel instability and relativistic electron beam transport in collisionless background plasma is developed. Beam electrons are modeled by macroparticles and the background plasma is represented by electron fluid. Conservation of generalized vorticity and quasineutrality of the plasma-beam system are used to simplify the governing equations. The method is suitable for modeling the nonlinear stages of collisionless beam-plasma interaction. A computationally efficient code based on this reduced description is developed and benchmarked against a standard particle-in-cell code. The full-scale two-dimensional numerical simulation of the Weibel instability saturation of a low-current electron beam is presented. Using the present approach, linear growth rates of the Weibel instability are derived for the cold and finite-temperature beams. © 2007 American Institute of Physics.

[DOI: 10.1063/1.2710812]

I. INTRODUCTION

High current electron and ion beams are transported through plasma in a variety of physical situations, ranging from astrophysical scenarios^{1–4} to inertial confinement fusion (ICF) and accelerator applications.^{5–9} Recently, the transport of relativistic electron beams through much denser background plasma has attracted considerable interest due to its relevance to the fast ignition (FI) scheme.⁸ In the FI scheme, the MeV relativistic electron beam produced by a high-intensity laser is transported through the much denser coronal plasma and deposited into the hot spot of the core pellet.⁵ Typically, the energy is deposited by the electron beam, although utilizing a proton beam has also been suggested.⁷ It is well known that the Weibel instability plays a particularly important role in the high-current beam-plasma interaction, because it leads to beam pinching and filamentation, beam and plasma heating, and generation of a strong magnetic field.^{10–13} Although the basics of electromagnetic beam-plasma instabilities were comprehensively developed long ago,^{13,14} the role of the Weibel instability in beam transport and stopping during FI is still a topic of active research.^{8,15–18}

In this paper, we present a reduced description of the Weibel instability for relativistic beams in much denser collisionless background plasmas. This regime is relevant to the astrophysical and FI (to a lesser degree) scenarios for which the beam energy is likely to be very high (corresponding to the relativistic gamma factor γ), and the beam density n_b is much smaller than the plasma density n_p . The combination of small n_b/n_p and large γ makes the growth rate of the Weibel instability, being proportional to the beam-plasma frequency

$\omega_b = \sqrt{4\pi e^2 n_b/m}$ and inversely proportional to $\sqrt{\gamma}$, much smaller than the electron plasma frequency $\omega_p = \sqrt{4\pi e^2 n_p/m}$ of the background plasma. Therefore, conventional particle-in-cell (PIC) codes that must resolve the electron plasma frequency are not best suited for modeling the long time behavior of the Weibel instability and its nonlinear stage. A review and a comparison of the standard PIC and various high-performance hybrid approaches, successfully implemented for various physical problems (but not similar to the presented approach), are given in Refs. 17 and 19–21. Considering that most of the beam energy depletion takes place during the nonlinear stage, development of an alternative code capable of simulating thousands of plasma periods over a reasonable period of time is desirable. To this end, we have developed and numerically implemented a two-dimensional (2D) model that does not require resolving the fast time scale. That is because our model kinetically evolves only the fast electron beam and not the background plasma treated as a fluid. High electron beam energy enables us to treat background and beam electrons as two separate species. The conservation of the generalized vorticity is used to relate the fluid plasma velocity to the self-generated magnetic field and the beam current while properly describing return current neutralization on a $\delta = c/\omega_p$ spatial scale. The background plasma is assumed collisionless in the present paper. Although in some cases collisions could be important for dense plasmas, one can still envision situations in which the role of collisions is not dominant. Indeed, for $\nu_{\text{coll}} \ll \gamma_\omega$, where ν_{coll} is the collision rate and γ_ω is the Weibel instability growth rate, the instability can be considered as collisionless with a good accuracy. For example, estimates from Ref. 22 for FI-

related plasmas yield $\nu_{\text{coll}}/\omega_p \sim 10^{-7} - 10^{-3}$ and $\nu_{\text{coll}}/\omega_p \ll \gamma_\omega/\omega_p \sim \sqrt{n_b/n_p}/\sqrt{\gamma} \sim 10^{-1} - 10^{-2}$ for $n_b/n_p \sim 10^{-1} - 10^{-3}$ and $\gamma \sim 2 - 6$. The entire beam-plasma system is treated as charge-neutral, which is well justified for the plasma which is much denser than the beam ($\omega_b \ll \omega_p$), as shown in Sec. II. Thus, the background plasma density is directly determined by the beam electron density. Although the main concern of this paper is the evolution of electron beams in background plasmas, the developed approach can also be easily modified to the case of propagation of ion beams in background plasmas.

II. PROBLEM FORMULATION AND DERIVATION OF FIELD AND PARTICLE EQUATIONS

Assumptions

We assume immobile ions forming a charge-neutralizing background. This assumption is valid when the ion response time is longer than the duration of the processes under consideration. The impact of finite ion mass on the development of the Weibel instability was reported, for example, in Refs. 26 and 27, where it was shown that the finite ion mass does not considerably change the instability behavior. The beam n_b and background plasma n_p densities are related to the ion density n_i by the quasineutrality assumption

$$n_p + n_b = n_i. \quad (1)$$

The assumption of quasineutrality is reasonable as long as $n_b \ll n_p$, because in this case the evolution of the electromagnetic Weibel instability proceeds slowly on the ω_p^{-1} time scale.¹⁴ The detailed analysis of the applicability of the quasineutrality assumption is given below.

Further in this paper, we concentrate only on the transverse spatial dynamics of the beam-plasma interaction. The effects of transverse-longitudinal plasma wave coupling are considered elsewhere^{14,24,25} (note, the longitudinal oscillations can be effectively damped by longitudinal beam temperature and/or by the steep plasma density gradient). Accordingly, we assume that the axial length of the electron beam is much larger than the inhomogeneity scale in the direction of propagation (z direction) and, therefore, we assume that all quantities of interest are z -independent. Then the magnetic field can be expressed as

$$\vec{B} = B_z \vec{e}_z - \vec{e}_z \times \nabla_{\perp} \psi, \quad (2)$$

where $\psi(x, y)$ is the longitudinal vector potential or poloidal field flux and B_z is the out-of-plane (toroidal) magnetic field.

Assuming that the electron plasma behaves as a cold collisionless fluid and satisfies the equation of motion

$$\frac{\partial \vec{v}_p}{\partial t} + (\vec{v}_p \cdot \vec{\nabla}) \vec{v}_p = -\frac{e}{m} \left(\vec{E} + \frac{\vec{v}_p \times \vec{B}}{c} \right), \quad (3)$$

taking the curl of it and using Faraday's law $\vec{\nabla} \times \vec{E} = -(1/c) \partial_t \vec{B}$, one can obtain the differential form of a conservation law²³ for generalized vorticity $\vec{\Omega} = \vec{\nabla} \times \vec{v}_p - e \vec{B}/mc$ in the form

$$\frac{\partial \vec{\Omega}}{\partial t} = \vec{\nabla} \times (\vec{v}_p \times \vec{\Omega}). \quad (4)$$

Assuming an initially quiescent plasma, one can obtain $\vec{\Omega} = 0$ for all times, and therefore

$$\vec{\nabla} \times \vec{v}_p = e \vec{B}/mc. \quad (5)$$

Equation (5) relates the axial plasma fluid velocity v_{pz} to the poloidal flux ψ and the transverse plasma velocity $\vec{v}_{p\perp}$ to the axial magnetic field B_z according to

$$v_{pz} = \frac{e}{mc} \psi, \quad (6)$$

and

$$\vec{\nabla}_{\perp} \times \vec{v}_{p\perp} = \frac{e}{mc} B_z \vec{e}_z. \quad (7)$$

III. DERIVATION OF FIELD EQUATIONS

Conservation of generalized vorticity significantly simplifies modeling electromagnetic beam-plasma instabilities. In conjunction with the quasineutrality assumption, it enables us to eliminate plasma electron equations of motion altogether. The only equations that need to be solved are equations for ψ , B_z , and equations of motion for the electron beam particles:

- (i) Knowing the beam current \vec{J}_b , fluid electron velocity \vec{v}_p from Eqs. (6) and (7), and plasma density n_p from quasineutrality, we can calculate the plasma electron current $\vec{J}_p = -en_p \vec{v}_p$ and the total electron current entering Ampere's law,

$$\vec{\nabla} \times \vec{B} = \frac{4\pi}{c} (\vec{J}_p + \vec{J}_b). \quad (8)$$

Note that, consistent with the quasineutrality assumption, the displacement current is neglected in Eq. (8). Projecting Eq. (8) on the z axis and using Eq. (6) yields the equation for the poloidal flux,

$$\nabla^2 \psi = \frac{\omega_p^2}{c^2} \psi - \frac{4\pi}{c} J_{bz}. \quad (9)$$

- (ii) The equation for B_z is obtained by taking the curl of the transverse part of Ampere's law in the form $-(\vec{e}_z \times \vec{\nabla} B_z)/n_p = -4\pi e \vec{v}_{p\perp}/c + 4\pi \vec{J}_{b\perp}/(cn_p)$, yielding

$$\left(\nabla^2 - \vec{\nabla} \ln n_p \cdot \vec{\nabla} - \frac{\omega_p^2}{c^2} \right) B_z = \frac{4\pi n_p}{c} \vec{\nabla} \cdot \left(\frac{\vec{e}_z \times \vec{J}_b}{n_p} \right). \quad (10)$$

- (iii) The electric field \vec{E} , to be used in the equation of motion for the beam particles, can be calculated using the plasma electron fluid equation of motion. The combination of the z component of Eq. (3) with Eq. (6) yields the axial electric field

$$E_z = -\frac{1}{c} \frac{\partial \psi}{\partial t}, \quad (11)$$

which also can be obtained from the transverse component of Faraday's law, $c\vec{\nabla} \times \vec{E} = -\partial_t \vec{B}$. The transverse part of Eq. (3) can be cast as the equation for \vec{E}_\perp ,

$$\vec{E}_\perp + \frac{v_{pz}}{c} \vec{e}_z \times \vec{B}_\perp = -\frac{m}{e} \left[\frac{\partial \vec{v}_{p\perp}}{\partial t} + \vec{\nabla} \left(\frac{\vec{v}_{p\perp}^2}{2} \right) \right], \quad (12)$$

where the $\vec{v}_{p\perp} \times \vec{e}_z B_z$ term is combined with the second term on the left-hand side (lhs) of Eq. (3) producing the second term on the right-hand side (rhs) of Eq. (12). What immediately distinguishes the equations for E_z and \vec{E}_\perp is that the latter is approximately consistent with the *inertialess* frozen-in law, $\vec{E} + \vec{v}_p \times \vec{B}/c = 0$, while the former is strikingly different, because electron inertia is retained in the longitudinal equation of motion for plasma electrons. This distinction between the longitudinal and transverse components of the electric field in initially unmagnetized plasma was pointed out in Ref. 23. Using Eq. (5), Eq. (12) can be recast as

$$\vec{E}_\perp = -\frac{e}{2mc^2} \vec{\nabla} \psi^2 - \frac{m}{e} \left[\frac{\partial \vec{v}_{p\perp}}{\partial t} + \vec{\nabla} \left(\frac{\vec{v}_{p\perp}^2}{2} \right) \right]. \quad (13)$$

The first term in Eq. (13) is due to the ponderomotive pressure of the transverse magnetic field on the plasma electrons while the second one is due to the electron inertia.

A. Equations of motion of the beam electrons

Once the electric and magnetic fields are determined, the equation of motion for the beam electrons is

$$\frac{d(\gamma \vec{v}_j)}{dt} = -\frac{e}{m} \left(\vec{E} + \frac{\vec{v}_j \times \vec{B}}{c} \right), \quad (14)$$

where the subscript j denotes the "jth" beam electron, and can be recast as

$$\frac{d(\gamma \vec{v}_{j\perp})}{dt} = -\frac{ev_{jz}}{mc} \vec{\nabla} \psi + \frac{e^2}{2m^2 c^2} \vec{\nabla} \psi^2 + \frac{\vec{F}_\perp}{m}, \quad (15)$$

where

$$\vec{F}_\perp \equiv \frac{eB_z}{c} \vec{e}_z \times \vec{v}_j + m \frac{\partial \vec{v}_{p\perp}}{\partial t} + m \vec{\nabla} \left(\frac{\vec{v}_{p\perp}^2}{2} \right) \quad (16)$$

and

$$\frac{d(\gamma \vec{v}_{jz})}{dt} = \frac{e}{mc} \left(\frac{\partial \psi}{\partial t} + \vec{v}_{j\perp} \cdot \vec{\nabla} \psi \right). \quad (17)$$

Equation (16) denotes the force originating from the axial magnetic field and plasma electron inertia in the transverse direction. Usually this force is much smaller than the first term on the rhs of Eq. (15), as shown below. Equation

(17) expresses the conservation of the z component of the canonical momentum of the beam electrons along their trajectories,

$$\gamma_j v_{jz} = \gamma_{j0} v_{jz0} + \frac{e}{mc} (\psi - \psi_{j0}), \quad (18)$$

and the initial conditions are $v_{jz}(t=0) = v_{jz0}$ and $\psi(\vec{x}_j(t=0)) = \psi_{j0}$.

Finally, the transverse electron fluid velocity $\vec{v}_{p\perp}$ is found from Ampere's law,

$$\vec{v}_{p\perp} = \frac{\vec{J}_{b\perp}}{en_p} + \frac{c}{4\pi en_p} \vec{e}_z \times \vec{\nabla} B_z. \quad (19)$$

The field equations, given by Eqs. (9) and (10), and equations of motion, given by Eqs. (15) and (18), form a closed system enabling the calculation of the complete dynamics of the beam-plasma interaction. Namely, fields are computed at each time step (after the beam particles are advanced), their density and currents are computed, and the background plasma density is calculated from Eq. (1).

The main advantages of the described approach over the existing PIC²¹ and hybrid Darwin-like models¹⁷ are as follows: (a) due to quasineutrality, we do not have to resolve the time scale $\Delta t = 1/\omega_p$ corresponding to the fast plasma oscillations; (b) the only spatial scale that needs to be resolved is the collisionless skin depth δ ; (c) the only quantities that are evolved in time are the beam position and velocities, not the background plasma parameters; and (d) there is no need to solve the advection-type fluid equation for plasma electrons, like in the hybrid Darwin approach. These features of the presented approach enable fast modeling of the long-time nonlinear behavior of the relativistic beams even on standard desktops, which can be of great help for various beam-plasma applications.

B. Justification of quasineutrality assumptions and force ordering

The applicability of the quasineutrality assumption can be analyzed as follows. Rewriting Eq. (13) for electric field with the help of Eq. (6) in the form $\vec{E}_\perp = -(\partial \vec{v}_{p\perp} / \partial t + \vec{\nabla} \vec{v}_p^2 / 2) m/e$, substituting it into Poisson's law,

$$\frac{1}{4\pi en_i} \vec{\nabla}_\perp \cdot \vec{E}_\perp = 1 - \frac{n_p + n_b}{n_i}, \quad (20)$$

and approximating the time and space derivatives as $\partial / \partial t \rightarrow \gamma_\omega$ and $\partial / \partial x_\perp \rightarrow 1/\delta$ (where γ_ω is the growth rate of the instability and δ is the characteristic transverse spatial scale) yields

$$1 - \frac{n_p + n_b}{n_i} \sim \left| \frac{\gamma_\omega v_{p\perp}}{\delta \omega_i^2} \right| + \left| \frac{v_p^2}{\delta^2 \omega_i^2} \right| \sim \left| \frac{\omega_b v_{p\perp}}{\omega_p c} \right| + \left| \frac{v_p^2}{c^2} \right|, \quad (21)$$

where $\omega_i^2 = 4\pi e^2 n_i / m$, and the estimates for the growth rate $\gamma_\omega \sim \omega_b$ (see the next section) and the smallest possible spatial scale $\delta \sim c/\omega_p$ [the scale of a homogenous solution of Eq. (9)] were used. Further, Eqs. (6) and (9) give the estimate

for the ratio of the axial plasma and beam velocities $v_{pz}/v_{bz} \sim \omega_b^2/\omega_p^2$, and Eqs. (7) and (10) yield the ratio of the transverse plasma and beam velocities $v_{p\perp}/v_{b\perp} \sim \omega_b^2/\omega_p^2$. Since for a relativistic beam $v_{bz} \sim c$, we find that $v_{p\perp} \ll v_{pz}$ and $v_p/c \ll 1$ as long as $\xi_1 \equiv v_{b\perp}/v_{bz} \ll 1$ and $\xi_2 \equiv \omega_b/\omega_p \ll 1$. Therefore, if $\xi_1, \xi_2 \ll 1$, then the quasineutrality assumption is well-justified,

$$1 - (n_b + n_p)/n_i \sim \xi_1 \xi_2^3 + \xi_2^4. \quad (22)$$

Also, rewriting Eq. (15) [using Eqs. (6) and (7)] in the form

$$\frac{d(\gamma \vec{v}_{j\perp})}{dt} = -v_{jz} \vec{\nabla} v_{pz} + (\vec{\nabla} \times \vec{v}_{p\perp}) \times \vec{v}_j + \frac{\partial \vec{v}_{e\perp}}{\partial t} + \frac{1}{2} \vec{\nabla} \vec{v}_e^2, \quad (23)$$

and using a similar reasoning, it can be easily shown that for $\xi_1, \xi_2 \ll 1$, the first term on the rhs of Eq. (23), corresponding to the Lorentz force exerted by the transverse magnetic field on the beam electrons, is much larger than all other terms, corresponding to the Lorentz force exerted by the axial magnetic field and the force of the inductive electric field, or,

$$|\vec{F}_\perp| \sim \frac{\xi_1 + \xi_1 \xi_2 + \xi_2^2}{\left| \frac{ev_{jz} \vec{\nabla} \psi}{mc} \right|}. \quad (24)$$

Therefore, the propagation of a relativistic electron beam into dense background plasma can also be approximately modeled using only the equation for the axial vector potential, Eq. (9), and the equations of transverse motion of the beam electrons in this potential, Eqs. (15), with $\vec{F}_\perp = 0$. The axial beam electron velocity v_{jz} is related to the axial vector potential through Eq. (18) and is approximately constant for $\xi_2 \ll 1$, because $\Delta v_{jz}/v_{jz} \sim \Delta v_{pz}/v_{jz} \sim v_{pz}/v_{jz} \sim \xi_2^2$, where Δ stands for the change along a beam particle trajectory.

Next, we demonstrate how the linear growth rate of the Weibel instability is recovered from this reduced model.

IV. LINEAR ANALYSIS OF THE WEIBEL INSTABILITY FROM THE REDUCED MODEL

To describe the linear stage of the Weibel instability for a cold beam-plasma system, it is assumed that an electron beam of density n_b propagates with velocity v_{bz} through the plasma with unperturbed density $n_{p0} = n_i \gg n_b$. Displacement of the plasma by the beam lowers the plasma density to $n_p = n_{p0} - n_b$. Also, we assume that the transverse width of the beam R_b is much larger than the collisionless skin depth $\delta = 1/k_p$. Equation (9) then yields the equilibrium poloidal flux function $\psi_0 = -(mc v_{bz}/e) n_b / (n_{p0} - n_b)$. Recalling that the longitudinal plasma fluid velocity is proportional to the poloidal flux, the return velocity of the electron fluid can be written as $v_{pz0} = -v_{bz} n_b / (n_{p0} - n_b)$. Consequently, in the limit of a very thick beam ($R_b \rightarrow \infty$), the corresponding electron plasma return current $J_r = -en_p v_{pz0}$ exactly cancels the beam current $J_b = -en_b v_{bz}$.

Assuming a small magnetic field perturbation $\delta\psi \propto e^{ik_\perp \cdot \vec{x}}$ superimposed on ψ_0 , the linearized Eq. (9) becomes

$$-(k_\perp^2 + k_p^2) \delta\psi = \frac{4\pi e^2 \delta n_p}{mc^2} \psi_0 + \frac{4\pi e}{c} (\delta v_{bz} n_b + \delta n_b v_{bz}), \quad (25)$$

where δn_p is the electron density perturbation, and $\delta n_b, \delta v_{bz}$ are the beam density and velocity perturbations, respectively. For the dense background plasma ($n_b \ll n_p$), the following relations hold: $\delta v_{bz} n_b \ll k_p^2 \delta\psi$ and $\delta n_p e \psi_0 / mc \ll \delta n_b v_{bz}$, which follow from direct substitution of the expressions for the potential and its equilibrium value and $\delta n_p = -\delta n_b$. Consequently, Eq. (25) can be rewritten as

$$-(k_\perp^2 + k_p^2) \delta\psi \approx +\frac{4\pi e}{c} v_{bz} \delta n_b. \quad (26)$$

The corresponding beam density perturbation, δn_b , can be expressed through $\delta\psi$ from the linearized beam equation of motion, Eq. (15), in the fluid form,

$$\frac{\partial \delta \vec{v}_{b\perp}}{\partial t} = -\frac{ev_{bz}}{\gamma mc} \vec{\nabla}_\perp \delta\psi, \quad (27)$$

and from the linearized continuity equation

$$\frac{\partial \delta n_b}{\partial t} = -n_b \vec{\nabla}_\perp \cdot \delta \vec{v}_{b\perp}. \quad (28)$$

Assuming that $\delta n_b \propto \exp(-i\omega t)$, taking the time derivative of Eq. (28), and substituting Eq. (27) yields

$$\frac{\delta n_b}{n_b} = \frac{k_\perp^2 c v_{bz}}{\omega^2} \frac{e \delta\psi}{\gamma mc^2}. \quad (29)$$

Substituting Eq. (29) into Eq. (26) produces the familiar¹⁰ dispersion relation for the Weibel instability of a cold electron beam propagating through cold plasma,

$$\omega^2 = -\frac{\omega_b^2}{\gamma} \frac{k_\perp^2}{k_\perp^2 + k_p^2} \frac{v_{bz}^2}{c^2}. \quad (30)$$

The above equation validates our reduced approach and shows that the Weibel instability is exponentially growing with the growth rate $\gamma_w \leq \omega_b v_{bz}/c \ll \omega_p$.

Note that the plasma temperature can be easily included in the above formalism as long as the plasma fluid thermal force term $-(\vec{\nabla} p)/n_p$ can be recast as a gradient, because this form does not violate the conservation of the generalized vorticity. The beam temperature is directly accounted for in the framework of a kinetic calculation. Arbitrary transverse and longitudinal temperatures of the beam can be modeled with the present approach. An example of the kinetic calculation of the linear stage of the Weibel instability for the initial waterbag-like distribution function for a warm beam is given in the Appendix.

V. NUMERICAL IMPLEMENTATION OF THE REDUCED MODEL AND SIMULATION RESULTS

The numerical algorithm for solving the system of Eqs. (9), (10), and (15), or its simplified version given by Eqs. (9) and (15) with $\vec{F}_\perp = 0$, consists of the following steps:

Initialization: Given the initial beam electron positions and momenta, the beam electron density and current are cal-

culated on the 2D (x, y) grid in the computational domain, according to the chosen weighting function.²¹ The coefficients in the equations for the fields ψ and B_z are calculated on the grid and the equations are solved on the grid. Both equations are second-order nonseparable (with coefficients depending on x, y) elliptic equations and are efficiently solved by the multigrid technique.²⁸

Simulation loop:

- (i) Once the beam electron positions, momenta, and fields are known on the grid, the transverse momenta and positions of the beam particles are evolved over one time step according to the equation of motions (15) using the fields weighted from the grid to the particles' positions.²¹ The second-order Runge-Kutta method for time integration was used.
- (ii) The beam density and current are recalculated using the new values for beam electron positions and transverse momenta as well as the nonevolved values of the axial beam momenta, and the equations for B_z and ψ are solved.
- (iii) Knowing the “predicted” values of ψ from (ii), Eq. (18) is solved for the “predicted” values of the axial beam electron momenta. The beam current is recalculated and the equations for the fields are solved for the “corrected” values. The “corrected” values of the $\gamma_j v_{zj}$ are also calculated. Step (iii) can be reiterated for higher accuracy (but usually a couple of iterations are sufficient).

A. Numerical simulation of the temporal dynamics of a low-current relativistic beam in background plasma

To demonstrate the effectiveness of our approach for modeling the long-time behavior of the Weibel instability, we have simulated the time evolution of a low-current ($I < I_A$, where $I_A = mc^3/e \times \gamma v_{bz}/c$ is the Alfvén current) electron beam propagating in a dense background plasma. The snapshots of the electron beam density at different times are presented in Fig. 1. Initially ($\omega_{p0}t=0$), the flat-top cylindrical electron beam with a radius $10c/\omega_{p0}$ and an initial beam-plasma density ratio $n_{b0}/n_{p0}=0.001$ are assumed. The initial axial (z direction) beam electron velocity is $0.885c$ and the initial transverse beam velocities are equally distributed in the range $\{-0.007c, 0.007c\}$, corresponding to water-bag distribution in the transverse directions. The computational domain was chosen as $32c/\omega_{p0} \times 32c/\omega_{p0}$ in the x, y directions, divided into 256×256 cells, and the number of the beam superparticles was 2.16×10^6 . The time behavior of the normalized energies of plasma (kinetic), magnetic and electric field energies, as well as the beam transverse energy are plotted in Fig. 2, where the straight line is the estimate for the instability growth rate (doubled) from Eq. (30), showing good agreement with the results of the full-scale numerical simulation.

Because the current of the finite-size beam cannot be exactly canceled by the plasma return current, as is seen from Eq. (9), the uncompensated beam current begins to drive the electromagnetic Weibel instability. This instability

initially manifests itself in pinching of the beam due to the radially inward Lorentz force (which must be larger than the thermal force; see the Appendix) with consequent ring formation ($\omega_{p0}t < 210$); see also Refs. 17 and 18. The transformation of the flat-top beam into the ring is due to the fact that initially the beam current is uncompensated by the return current mainly at the beam edge. Later on, as the first formed ring is pushed inwards, the second ring is created at the beam edge and the beam starts to break up into numerous filaments ($\omega_{p0}t = 310$). Subsequently, the filaments merge and finally ($\omega_{p0}t = 460$) coalesce into a single pulsating filament, with $n_b/n_{b0} \sim 100$ and the instability saturates.

The instability saturation occurs when the beam electrons acquire the radial velocity large enough to traverse the filament of characteristic size R_b by the time corresponding to the characteristic time of the instability growth $1/\gamma_\omega$. When this condition is met, the beam electrons start to sample the Lorentz force in both the inward and outward radial directions as they oscillate. This simple estimate results in

$$R_b \sim \frac{v_{bz}}{\gamma_\omega} \times \frac{\Omega_c}{\gamma_\omega}, \quad (31)$$

where $\Omega_c = eB/(\gamma mc)$ is the cyclotron frequency of the transverse magnetic field. This condition is equivalent to the earlier derived condition,^{11,13} which equated the rate of the instability growth to the frequency of oscillation of the magnetically trapped beam electrons (in our case electrons bounce in the poloidal flux of the filament). From this estimate (assuming $R_b \sim 1/k_p$), the fraction of the energy transferred to the magnetic field can be evaluated as follows:

$$\frac{E_{\text{magn}}}{E_{\text{beam}}} \sim \frac{B^2/8\pi}{(\gamma-1)mc^2 n_b} \sim \frac{1}{8(\gamma-1)} \frac{n_b v_{bz}^2}{n_e c^2} \sim \frac{\gamma}{2(\gamma-1)} \frac{I}{I_A}. \quad (32)$$

For our simulations, the normalized beam density of the compressed single filament at saturation is $n_b/n_e \sim 0.1$, as is seen from Fig. 1, and the above formula yields $E_{\text{magn}}/E_{\text{beam}} \sim 0.001$, which is roughly in agreement with the results of our numerical simulations, shown in Fig. 2. After saturation, because of the beam overfocusing, the peak energy conversion overshoots the saturation value given by Eq. (32). Subsequent nonlinear oscillations of the filament radius are reflected in the oscillations of the magnetic and plasma energies shown in Fig. 2.

Note that the present qualitative description of the saturation mechanism is only valid for low-current beams with total current less than the Alfvén current. The detailed analysis of the saturation of the Weibel instability and long-time nonlinear beam-plasma behavior is the important topic, which still needs further elaboration, and will be presented in a forthcoming publication.

B. Benchmarking with the LSP PIC code

For benchmarking purposes, the LSP PIC code²⁹ is used in order to provide comparison to the numerical simulation described above. The 2D (r, θ) PIC simulation domain ex-

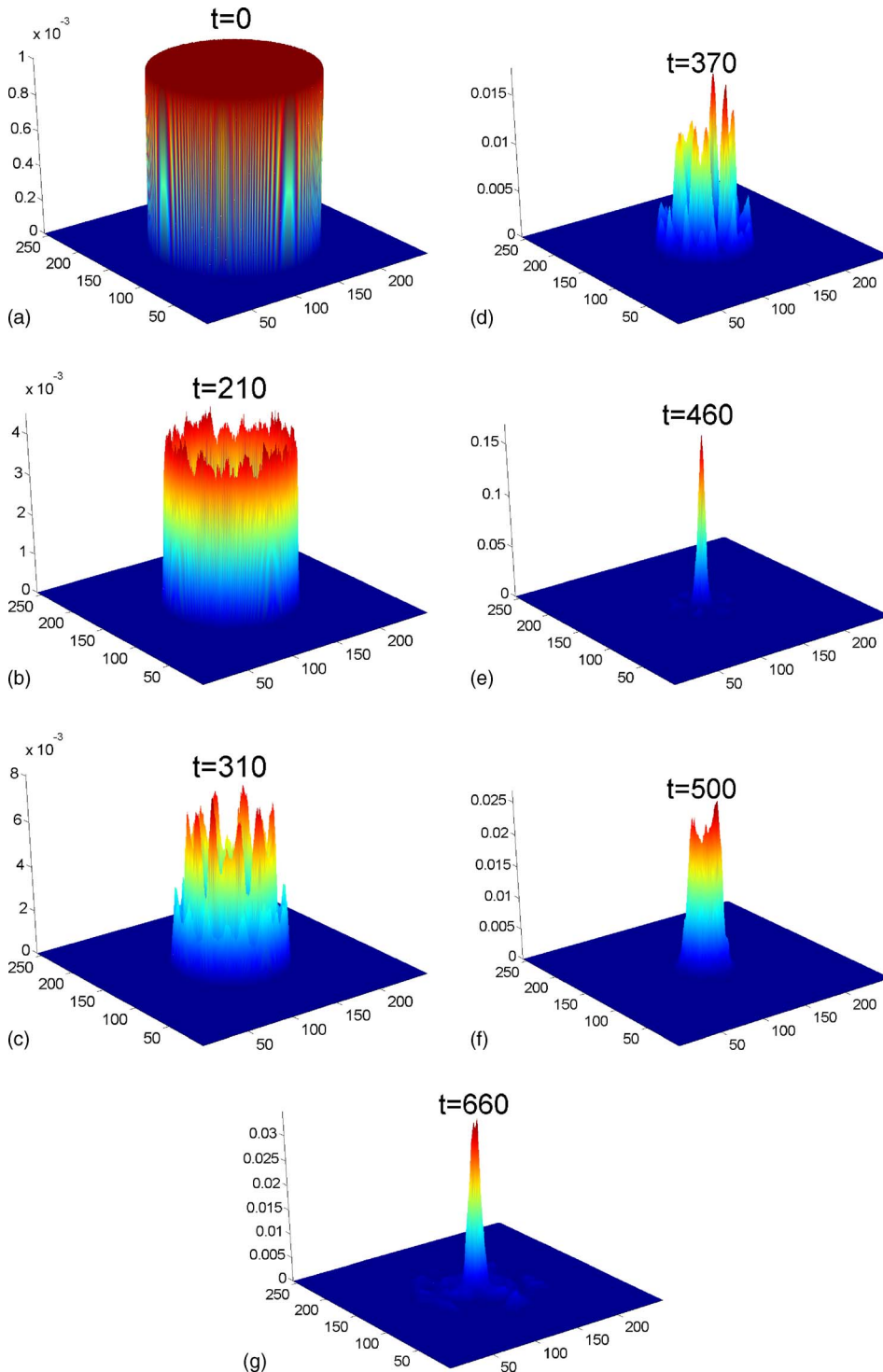


FIG. 1. (Color online) The temporal evolution of the electron beam density normalized to the ion density. z axis, normalized beam density; x,y axes, spatial grid. Snapshots at different normalized times $\omega_{pe}t$ are shown: (a) $t=0$, initial beam density; (b) $t=210, 310$, and 370 , “ring” formation with subsequent filamentation; (c) $t=460$, maximal compression corresponding to instability saturation; (d) $t=500$ and 660 , post-saturational radial oscillation of the beam. Cold electron beam with $n_b/n_{p0}=0.001$ and $v_{bz}/c=0.885$ was assumed.

tends from $r=0$ to $r=32c/\omega_{pe}$ and from $\theta=0$ to $\theta=2\pi$ rad with grid spacings $\Delta r=0.15c/\omega_{pe}$ and $\Delta\theta=0.1$ rad. Periodic boundary conditions are enforced in the θ direction. The electromagnetic field equations are solved implicitly in order to increase the time step of the simulation by a factor of 10 relative to the Courant condition; the time step satisfies $\omega_{pe}\Delta t=0.14$.

All particles in the LSP simulation are pushed by an explicit particle mover using the well-known “leap-frog” technique, which splits the electric field push into two halves between the magnetic field rotation. The background plasma

particles are treated as fluid species, whereas the electron beam particles are treated kinetically, as in the reduced model presented in this paper. An energy-conserving particle push that is not susceptible to the so-called Debye-length numerical instability is used for all species. Therefore, a grid spacing that under-resolves the Debye length is allowed while good energy conservation is maintained. Also, a cloud-in-cell method that reduces noise due to discrete particle effects is employed in the PIC interpolation scheme.

As in the numerical simulation presented in Sec. V A, a flat-top cylindrical beam with radius $10c/\omega_{pe}$ is injected

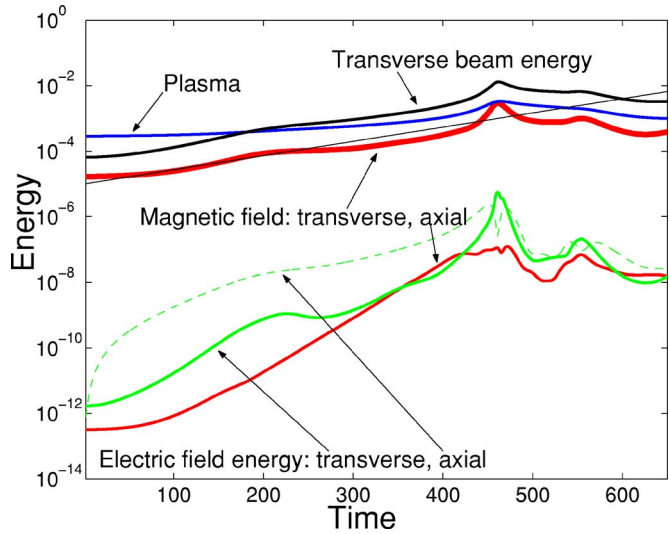


FIG. 2. (Color online) Time development of normalized energies of plasma, magnetic (transverse and axial) and electric (transverse and axial) fields, and beam [transverse, $\sum_j(\gamma_{j\perp}-1)mc^2$]. All energies are normalized on the axial beam energy $\sum_j(\gamma_{jz}-1)mc^2$. Straight line, the average initial growth rate from Eq. (30). Parameters as in Fig. 1. Time is normalized to ω_{p0}^{-1} .

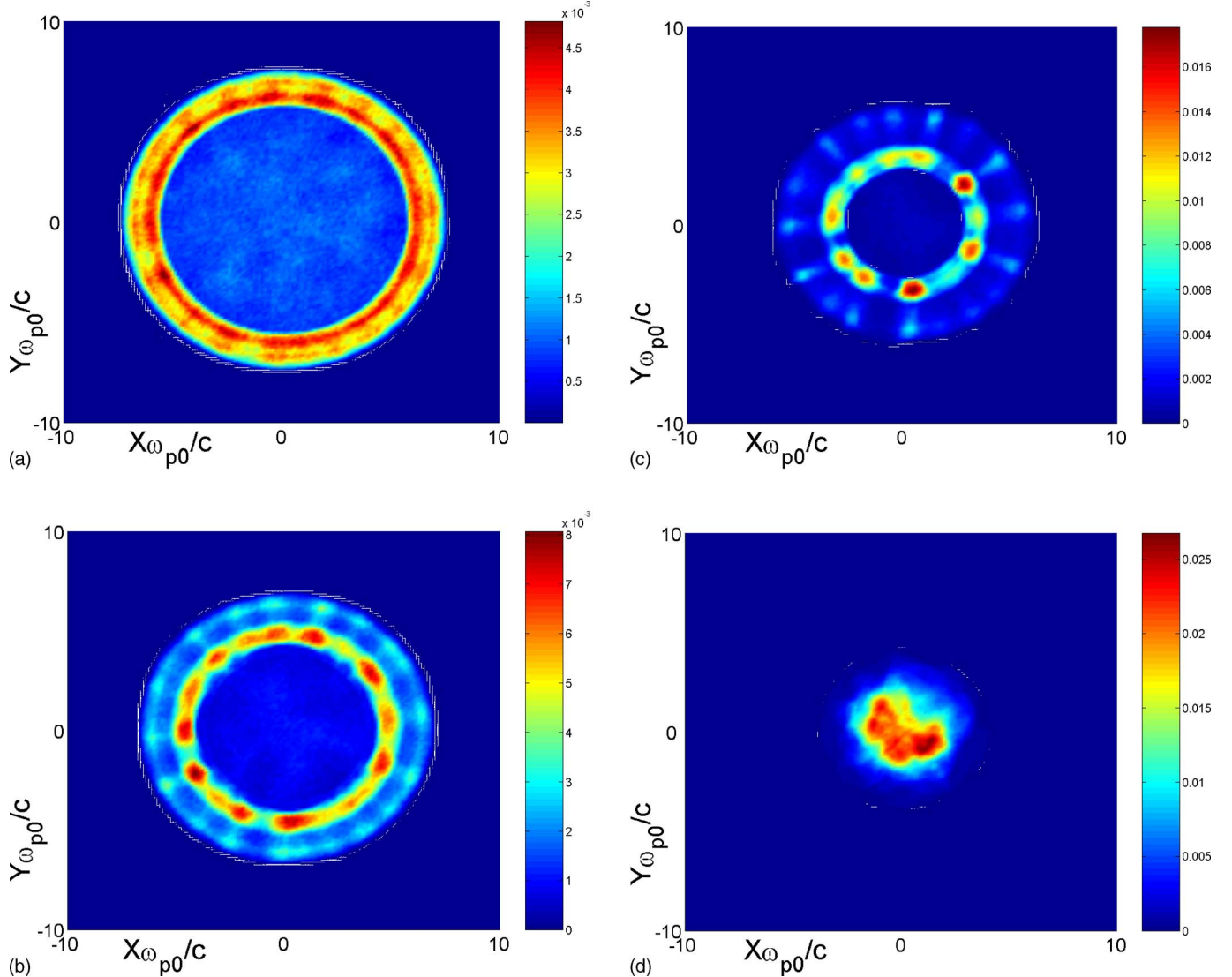


FIG. 3. (Color online) The electron beam density normalized to the ion density simulated by the approach of this paper. Time snapshots: (a) $\omega_{p0}t=220$, (b) $\omega_{p0}t=320$, (c) $\omega_{p0}t=380$, and (d) $\omega_{p0}t=490$.

into the simulation with an axial directed velocity of $\beta_z = 0.885$ (without spread) using 90 beam particles per cell. The initial electron beam density relative to the initial background plasma density is 10^{-3} and the initial transverse beam velocities are equally distributed between $\beta = [-0.007, +0.007]$.

The electron beam density plots simulated by the reduced approach presented in this paper are shown in Fig. 3 (total run time 30 min), and the results from the hybrid PIC treatment in LSP simulations (total run time 10 h), using fluid plasma species with kinetic electron beam particles, are shown in Fig. 4. Both codes were run on similar desktop computers (Pentium 4). Good agreement between the two models is evident. Both simulations show radial compression and filamentation of the electron beam due to the electromagnetic Weibel instability. The fact that the LSP simulated filaments have more structure is attributable to intrinsic properties of PIC codes. Some amount of numerical noise inevitably contributes to the seeding of the instability, and this noise can be quite different for different codes. Nevertheless,

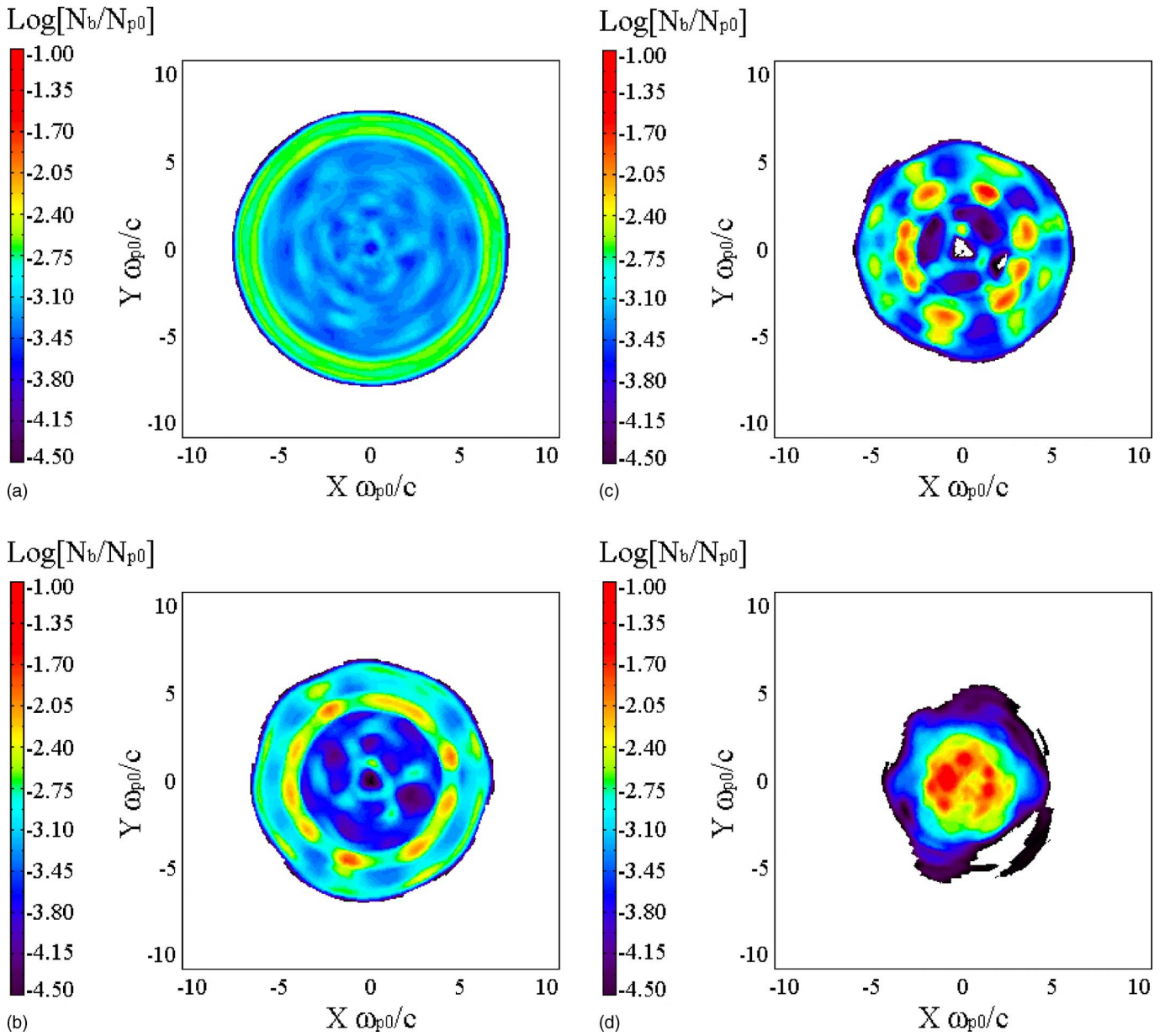


FIG. 4. (Color online) The electron beam density normalized to the ion density, simulated by the LSP PIC code. Parameters: as in Figs. 1–3.

we consider the agreement between the LSP and our simulations to be very good: all stages of the instability are reproduced by both codes very similarly.

VI. CONCLUSIONS

We have developed a reduced description of the Weibel instability for relativistic beams in much denser collisionless plasmas. When the beam density is much smaller than the plasma density and the beam energy is high, the growth rate of the Weibel instability is small, placing stringent computational resource requirements on the conventional PIC model. We have developed and numerically implemented a 2D reduced model that does not require resolution of the plasma period and evolves only the fields and beam electrons. In our approach, the plasma is treated as a fluid and the beam as kinetic macroparticles. The quasineutrality assumption used together with the conservation of generalized vorticity en-

ables us to eliminate plasma electron fluid quantities altogether. Using this model, we were able to model long-time beam-plasma dynamics, paying special attention to the details of the nonlinear stage of the Weibel instability, such as filamentation, instability saturation, and post-saturation field and energy oscillations. The validity and computational efficiency of our code was verified by comparisons with the first-principles LSP PIC code. Further work will incorporate finite plasma temperature and resistivity effects.

APPENDIX: KINETIC CALCULATION OF THE LINEAR GROWTH RATE OF THE WEIBEL INSTABILITY

Here we apply the reduced description of the Weibel instability in dense plasma developed in Sec. III to derive the kinetic growth rate for a specific (water-bag) distribution function of a warm electron beam.

The linearized relativistic Vlasov equations reads

$$\frac{\partial f_1}{\partial t} + \frac{\vec{p}}{m\gamma} \frac{\partial f_1}{\partial \vec{x}} - \frac{e}{cm\gamma} \vec{p} \times \vec{B} \frac{\partial f_0}{\partial \vec{p}} = 0, \quad (\text{A1})$$

where the electric field given by Eqs. (11) and (12) is neglected for $|\psi| \ll 1$. The unperturbed distribution function for the warm relativistic electron beam is assumed in the following form:

$$f_0(p_x, p_y, p_z) = \frac{n_b}{\pi P_{\perp}^2} \Theta(P_{\perp} - \sqrt{p_x^2 + p_y^2}) \delta(p_z - P_z), \quad (\text{A2})$$

where $\Theta(x)=0$ or 1, respectively, for $x < 0$ or $x \geq 0$.

Representing the perturbed part of the distribution function as $f_1 = \delta f_1 e^{i(k_x x + k_y y - \omega t)}$ and the same for all field quantities, the solution of Eq. (A1) for $p_z \gg p_x, p_y$ is given by

$$\delta f_1 = -\frac{e}{c} \frac{k_x \frac{\partial}{\partial p_x} + k_y \frac{\partial}{\partial p_y}}{p_z \delta \psi - m\gamma\omega - k_x p_x + k_y p_y} f_0, \quad (\text{A3})$$

where $B_x = \partial \delta \psi / \partial y$ and $B_y = -\partial \delta \psi / \partial x$ were used.

Using Eqs. (A2) and (A3), the axial beam current can be expressed as

$$\delta j_{bz} = \frac{e^2 n_b P_z^2}{cm\pi P_{\perp}^2} \delta \psi \int \frac{dp_x dp_y \vec{k}_{\perp} \cdot \vec{\nabla}_p \Theta(P_{\perp} - \sqrt{p_x^2 + p_y^2})}{\gamma m\gamma\omega - \vec{k}_{\perp} \cdot \vec{p}}, \quad (\text{A4})$$

where the integration over p_z has been performed and $\gamma = \sqrt{p_x^2 + p_y^2 + P_z^2}$.

To integrate the above equation, it is convenient to express the scalar products in the numerator and denominator in polar coordinates ($p_x = p \cos \phi, p_y = p \sin \phi$ and $k_x = k \cos \vartheta, k_y = k \sin \vartheta$) as $\vec{k}_{\perp} \cdot \vec{\nabla}_p = k \cos \theta \partial/\partial r + k/p \sin \theta \partial/\partial \theta$ and $\vec{k}_{\perp} \cdot \vec{p} = kp \cos \theta$ with $\theta = \vartheta - \phi$. Using the relation $\int_0^\infty dp f(p) d\Theta(c-p)/dp = -f(c)$, the beam axial current can be rewritten as

$$\delta j_{bz} = -\frac{e^2 n_b P_z^2}{cm^2 \pi P_{\perp}^2} \frac{k}{\omega \gamma^2} \delta \psi \int_0^{2\pi} d\theta \frac{\cos \theta}{1 - \frac{k P_{\perp}}{\omega m \gamma} \cos \theta}, \quad (\text{A5})$$

where $\gamma \equiv \gamma(P_{\perp}, P_z)$. For complex ω , the integrand is nonsingular and the simple integration yields

$$\delta j_{bz} = -\frac{e^2 n_b P_z^2}{cm P_{\perp}^2} \frac{2}{\gamma} \delta \psi \left[\frac{1}{\sqrt{1 - \frac{k^2 P_{\perp}^2}{\omega^2 m^2 \gamma^2}}} - 1 \right], \quad (\text{A6})$$

where $u = P_z/(m\gamma)$ and $V_{\perp} = P_{\perp}/(m\gamma)$.

Finally, substitution of the beam axial current into the linearized equation for the poloidal field flux

$$\nabla^2 \delta \psi - \frac{\omega_e^2}{c^2} \delta \psi \approx -\frac{4\pi}{c} \delta j_{bz} \quad (\text{A7})$$

leads to the dispersion equation yielding the linear kinetic growth rate of the instability $\gamma_{\omega} = -\text{Im}(\omega)$,

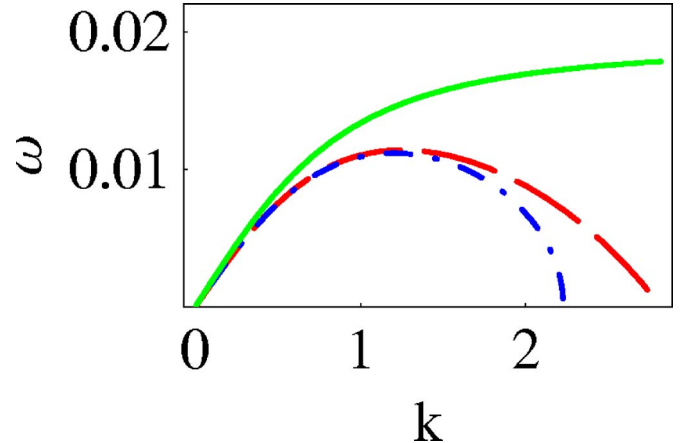


FIG. 5. (Color online) The dispersion curves for the cold beam (solid line) and warm beam [dashed line, Eq. (A11); dash-dotted line, Eq. (A9)]. Parameters are as in Fig. 1.

$$k_{\perp}^2 + \frac{\omega_e^2}{c^2} = -2 \frac{\omega_b^2}{\gamma} \frac{u^2}{c^2 V_{\perp}^2} \left[\frac{1}{\sqrt{1 - \frac{k^2}{\omega^2} V_{\perp}^2}} - 1 \right]. \quad (\text{A8})$$

The solution of this equation is

$$\omega^2 = -\frac{1}{\gamma} \frac{k^2}{k^2 + \frac{\omega_e^2}{c^2}} \left[\frac{\gamma \left(k^2 + \frac{\omega_e^2}{c^2} \right) V_{\perp}^2 - 2 \frac{u^2}{c^2} \omega_b^2}{\gamma \left(k^2 + \frac{\omega_e^2}{c^2} \right) V_{\perp}^2 - 4 \frac{u^2}{c^2} \omega_b^2} \right]^2. \quad (\text{A9})$$

Expanding the above equation to zeroth order in V_{\perp}^2 yields the conventional dispersion relation for the Weibel instability of a cold beam given by Eq. (30),

$$\omega^2 = -\frac{\omega_b^2 u^2}{\gamma} \frac{k^2}{k^2 + \omega_e^2/c^2}. \quad (\text{A10})$$

The first order in V_{\perp}^2 expansion yields the lowest-order temperature correction (see also Refs. 14 and 17),

$$\omega^2 = -\frac{\omega_b^2 u^2}{\gamma} \frac{k^2}{k^2 + \omega_e^2/c^2} + \frac{3}{4} V_{\perp}^2 k^2. \quad (\text{A11})$$

Analysis of the dispersion equation (A9) yields the parameters range for which the Weibel instability exponentially grows (see Fig. 5). As is seen from Eq. (A9), the frequency is complex if the denominator is positive, yielding the upper bound for the growing wave vectors for warm plasmas,

$$\frac{k_{\max}}{k_p} = \sqrt{\frac{4}{\gamma} \frac{u^2}{V_{\perp}^2} \frac{\omega_b^2}{\omega_e^2} - 1}. \quad (\text{A12})$$

Now, it is seen that, although all modes corresponding to all spatial scales participate in the beam pinching for a cold beam, the only modes that grow for the warm beam have a characteristic size larger than $1/k_{\max}$. Also, as k_{\max} must be positive, Eq. (A10) produces the condition on the upper possible beam temperature supporting the unstable modes,

$$\frac{V_{\perp}}{u} < \frac{2}{\sqrt{\gamma}} \sqrt{\frac{n_b}{n_e}}. \quad (\text{A13})$$

If the above equation is not satisfied, then the thermal pressure force of the beam electrons is larger than the Lorentz force exerted by the transverse magnetic field on the beam. Therefore, instead of pinching, the beam spreads transversely.

- ¹M. V. Medvedev and A. Loeb, *Astrophys. J.* **526**, 697 (1999).
- ²L. O. Silva, R. A. Fonseca, J. W. Tonge, W. B. Mori, and J. M. Dawson, *Phys. Plasmas* **10**, 1979 (2003).
- ³R. Schlickeiser and P. K. Shukla, *Astrophys. J. Lett.* **599**, L57 (2003).
- ⁴A. Gruzinov, *Astrophys. J. Lett.* **563**, L15 (2001).
- ⁵M. Tabak, J. Hammer, M. Glinsky, W. L. Kruer, S. C. Wilks, J. Woodworth, E. M. Campbell, and M. Perry, *Phys. Plasmas* **1**, 1626 (1994).
- ⁶J. Meyer-ter-Vehn, *Plasma Phys. Controlled Fusion* **43**, A113 (2001).
- ⁷M. Roth, T. E. Cowan, M. H. Key *et al.*, *Phys. Rev. Lett.* **86**, 436 (2001).
- ⁸L. O. Silva, R. A. Fonseca, J. W. Tonge, W. B. Mori, and J. M. Dawson, *Phys. Plasmas* **9**, 2458 (2002).
- ⁹E. A. Startsev and R. C. Davidson, *Phys. Plasmas* **10**, 4829 (2003).
- ¹⁰E. W. Weibel, *Phys. Rev. Lett.* **2**, 83 (1959).
- ¹¹R. L. Morse and C. W. Nielson, *Phys. Fluids* **14**, 830 (1971).
- ¹²R. Lee and M. Lampe, *Phys. Rev. Lett.* **31**, 1390 (1973).
- ¹³R. C. Davidson, D. A. Hammer, I. Haber, and C. E. Wagner, *Phys. Fluids* **15**, 317 (1972).
- ¹⁴A. I. Ahiezer and I. A. Ahiezer, *Plasma Electrodynamics* (Pergamon, New York, 1974).
- ¹⁵F. Pegoraro, S. V. Bulanov, F. Califano *et al.*, *Plasma Phys. Controlled Fusion* **39**, B261 (1997).
- ¹⁶M. Honda, J. Meyer-ter-Vehn, and A. Pukhov, *Phys. Plasmas* **7**, 1302 (2000).
- ¹⁷T. Taguchi, T. M. Antonsen, Jr., C. S. Liu, and K. Mima, *Phys. Rev. Lett.* **86**, 5055 (2001).
- ¹⁸M. C. Firpo, A. F. Lifschitz, E. Lefebvre, and C. Deutsch, *Phys. Rev. Lett.* **96**, 115004 (2006).
- ¹⁹E. V. Belova, R. C. Davidson, H. Ji, and M. Jamada, *Phys. Plasmas* **11**, 2523 (2004).
- ²⁰L. Gremillet, G. Bonnaud, and F. Amiranoff, *Phys. Plasmas* **9**, 941 (2002).
- ²¹C. K. Birdsall and A. B. Langdon, *Plasma Physics via Computer Simulations* (McGraw-Hill, New York, 1981).
- ²²J. M. Hill, M. H. Key, S. P. Hatchett, and R. R. Freeman, *Phys. Plasmas* **12**, 082304 (2005).
- ²³I. D. Kaganovich, G. Shvets, E. Startsev, and R. C. Davidson, *Phys. Plasmas* **8**, 4180 (2001).
- ²⁴M. Tzoufras, C. Ren, F. S. Tsung, J. W. Tonge, W. B. Mori, M. Fiore, R. A. Fonseca, and L. O. Silva, *Phys. Rev. Lett.* **96**, 105002 (2006).
- ²⁵A. Bret, M. C. Firpo, and C. Deutsch, *Phys. Rev. Lett.* **94**, 115002 (2005).
- ²⁶R. C. Davidson, I. Kaganovich, and E. A. Startsev, *Nucl. Instrum. Methods Phys. Res. A* (submitted).
- ²⁷T. Matsumoto, T. Taguchi, and K. Mima, *Phys. Plasmas* **13**, 052701 (2006).
- ²⁸J. Adams, *Appl. Math. Comput.* **34**, 113 (1989).
- ²⁹LSP is a software product of ATK Mission Research, Albuquerque, NM 87110.